NRL Report 7566

UNCLASSIFIED

Resolution of Point Scatterers by Hard-Limited Synthetic Aperture Radar

GEORGE C. GEORGES

Aerospace Radar Branch
Radar Division

June 25, 1973

NAVAL RESEARCH LABORATORY
Washington, D.C.

Approved for public release; distribution unlimited.

UNCLASSIFIED

CONTENTS

Abstract ii
Authorization ii

INTRODUCTION 1

FORMULATION OF THE MODEL 2

Description of the Radar System 2
Derivation of the Received Signal 3
Generation of the Signal Film and Optical Processing 6

EVALUATION OF THE MAP FUNCTION 7

Effect of Random Phase Fluctuations 7
Resolution of Weak Targets in the Presence of a Strong Target 8
Special Case of Two Targets 11

COMPUTER RESULTS 12

Definition of Parameters 12
Single Target Per Antenna Beamwidth 14
Two Targets Per Antenna Beamwidth 15
Three Targets Per Antenna Beamwidth 17
Ten Targets Per Antenna Beamwidth 18
Resolving Uniform Arrangements of Many Targets 21

SUMMARY 23

REFERENCES 25

APPENDIX A—Computer Program to Evaluate $v_s(\tau)$ and $m(\tau)$ 26

ABSTRACT

Image maps of collections of point targets are investigated for hard-limited synthetic aperture radar application. Some aspects of hard-limiting, such as image suppression and spurious image generation, are derived under specialized weak-scatterer assumptions. Also, the effect of random variations of target phases on synthetic aperture resolution are studied. Such phase deviations are used to model random motions of target locations and, as expected, it is found that they hinder one's ability to resolve the targets. Graphical plots of some point-target arrangements are presented to illustrate effects of hard limiting and random phase variations. Numerical calculations are used to verify the approximate weak-scatterer theory and to study more general cases such as problems involving more than one strong target which are not readily solved by analytical means.

A simple averaging procedure is devised which predicts many aspects of the more accurate numerical results, and the procedure may perhaps be employed in future investigations of mapping continuum scattering surfaces rather than point scatterers.

AUTHORIZATION

NRL Problem R07-02
Project RR 021-01-41-5550

Manuscript Submitted February 26, 1973.

UNCLASSIFIED

RESOLUTION OF POINT SCATTERERS BY HARD-LIMITED SYNTHETIC APERTURE RADAR

INTRODUCTION

As is well-known, synthetic aperture radar is an effective high-resolution-radar technique for airborne mapping systems [1]. By such means, one can ideally resolve scale lengths as small as the dimension of the radar antenna [2]. However, higher resolution systems require increasingly longer processing of doppler phase histories of the return signal. Thus high-resolution synthetic aperture radar requires storage of a large number of samples of the return signal. To simplify this problem, the dynamic range of returned voltage is reduced by hard-limiting [3a] the signal; prior to storage the return signal $v_r(t)$ arriving at the radar receiver is passed through a high-gain (or hard-limiter) circuit to obtain the desired hard-limited return signal as

$$v_H(t) \equiv h(v_r) = 1, \text{ if } v_r(t) > 0, \tag{1a}$$

$$= -1 \text{ if } v_r(t) < 0. \tag{1b}$$

As will be shown, $v_H(t)$ retains information on the structure of the actual return voltage $v_r(t)$ and can thus be used to resolve the targets. Since $v_H(t)$ can assume only two discrete levels, processing $v_H(t)$ is obviously much easier than processing $v_r(t)$.

This report will consider how hard-limiting of the received signal affects the performance of synthetic aperture mapping systems. As will be shown, the mapping process requires a separation of various frequency components in $v_H(t)$. However, the hard-limiting operation introduces nonlinearities in the process and hence complicates this analysis. For example the nonlinear aspect of hard-limited signals precludes derivation of an exact analytical expression for the frequency content of $v_H(t)$. Various approximate analyses have been derived by other authors [3a-6], but due to inherent weak-scatterer assumptions these derivations cannot treat problems involving more than one strong target. By modeling the synthetic aperture system on a digital computer, some interesting results on resolution of target configurations are obtained that cannot be easily analyzed in closed form. Also approximate expressions of the effects of random phase fluctuations on target resolution are derived and compared with numerical results.

The next section formulates an appropriate point scatterer model for numerical analysis of the problem, and results are presented in graphical form in the fourth section. In the third section, based on these computer results, some approximate analytical expressions are derived for target resolution in the presence of random phase fluctuations. This point-scatterer formulation is evidently appropriate for analyzing hard-limited synthetic aperture mapping of discrete scatterers, such as collections of localized objects which may be considered as point reflectors. An attempt is made to model the mapping of surfaces with a continuous distribution of scatterers, such as mapping of oil slicks over water waves [7], by prescribing a step discontinuity in scattering intensity of an otherwise uniform collection of point scatterers. As will be discussed, the effect of hard-limiting

is to cause a spike (or differentiation of the step discontinuity) to appear in the corresponding image map. Although this treatment of continuous scattering surfaces agrees with experimental results [7], a more deductive treatment of this problem would require consideration of the average radar-scattering cross section for the ocean surface [8], rather than a point scatterer formulation. This analysis is a subject for future research and will be treated in another report.

FORMULATION OF THE MODEL

Description of the Radar System

To arrive at an appropriate mathematical model for the synthetic aperture radar system, the following operational system is assumed [3b].

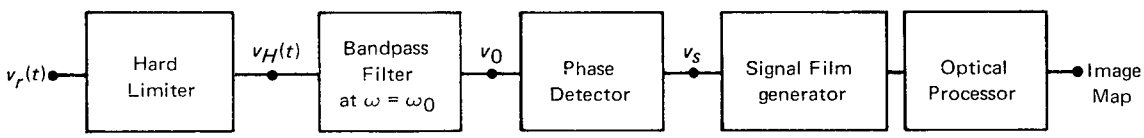

The desired mathematical expression for v_s is obtained by extracting the ω_0 frequency component from the Fourier representation of $v_H(t)$ and, in turn, mixing the resultant band-limited signal (v_0) through the phase detector circuit. The analysis of this process may be derived as follows [3]. Let us represent the received signal in terms of amplitude and phase quantities $A(t)$ and $\Phi(t)$ as

$$v_r(t) = A \cos(\omega t + \Phi). \tag{2}$$

As indicated by Eqs. (1), the hard-limiter circuit is assumed to be an instantaneous function of $v_H(t)$. Hence we may write the Fourier representation for $v_H(t)$ as

$$v_H(t) = h(v_r) = \int_{-\infty}^{\infty} e^{-i\omega v_r} H(\omega) \frac{d\omega}{2\pi}, \tag{3}$$

where, by Eq. (1), $H(\omega) = 2/-i\omega$, $Im\omega > 0$. Substituting Eq. (2) into Eq. (3), we find

$$v_H(t) = -2 \int_{-\infty}^{\infty} \frac{e^{-i\omega' A \cos(\omega t + \Phi)}}{i\omega'} \frac{d\omega'}{2\pi}$$

$$= 2i \sum_{m=0}^{\infty} -\epsilon_m i^m \cos m(\omega t + \Phi) \int_{-\infty}^{\infty} \frac{J_m(\omega' A)}{\omega'} \frac{d\omega'}{2\pi},$$

where

$$\epsilon_m = 1, \text{ if } m = 0,$$
$$= 2, \text{ if } m \neq 0.$$

UNCLASSIFIED

Hence

$$v_H(t) = \frac{4}{\pi} \sum_{\substack{m=1 \\ m \text{ odd}}}^{\infty} \frac{(-1)^{m+1}}{m} \cos m(\omega t + \Phi). \tag{4}$$

The filtered output v_0 is then found by extracting the $m = 1$ term from Eq. (4) as

$$v_0(t) = \frac{4}{\pi} \cos(\omega t + \Phi).$$

The ωt phase component is then removed by processing $v_0(t)$ in the phase detector circuit to obtain

$$v_s(t) = \cos \Phi. \tag{5}$$

In subsequent analysis we shall generate resolution maps of radar targets by processing $v_s(t)$ in a manner appropriate to the optical processor.

Derivation of the Received signal

In deriving the returned signal, we picture a discrete set of point targets and assume that $v_r(t)$ in Eq. (2) can be expressed as a superposition of returns from the individual point scatterers. The coordinate system shown in Fig. 1 will be used in our analysis.

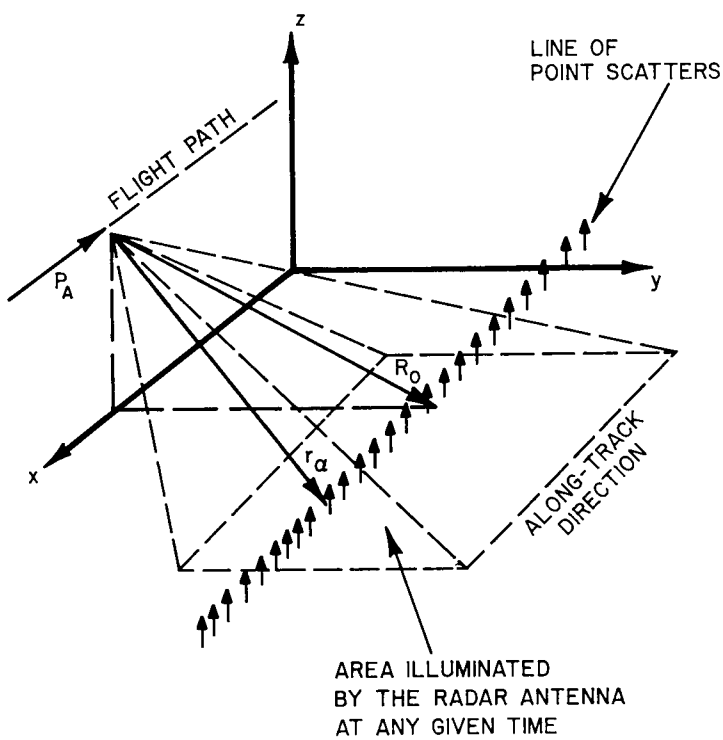

Fig. 1—Configuration of point targets relative to the aircraft and radar beam

In conventional radar, targets are resolved along the range direction r_α by range-gating the returned signal. In this report we shall be concerned with processing the returned signal from targets along the x direction at a fixed range from the aircraft flight path. At any given time of radar observation, the distance from the radar antenna to say the αth scatterer is designated by

$$r_\alpha = \sqrt{R_0^2 + (x - x_\alpha)^2}\,, \tag{6a}$$

where x is the along-track location of the aircraft, x_α is the along-track location of the αth scatterer and R_0 is the minimum distance from P_A to the along-track line of targets. If ${R_0}^2 >> (x - x_\alpha)^2$, r_α may be approximated as

$$r_\alpha \approx R_0 + \frac{(x - x_\alpha)^2}{2R_0}$$

$$= R_0 + \frac{v^2}{2R_0}\,(t - t_\alpha)^2\,, \tag{6b}$$

where v is the aircraft speed along the x direction.

Each scatterer will be assumed to radiate a spherical wave whose field intensity E_α at point P_A is linearly proportional to the incident field intensity at the scatterer as*

$$E_\alpha(P_A) = \frac{a_\alpha E_{inc}(r_\alpha) e^{i(\omega t - k r_\alpha + \phi_\alpha)}}{r_\alpha}$$

where k is the free-space wave number, ϕ_α is a prescribed phase factor, and a_α is a proportionality constant depending on the scattering cross section of the αth scatterer. For simplicity we neglect the directional antenna gain variations within the illuminated region and assume

$$E_{inc}(r_\alpha) \propto \frac{e^{-ikr_\alpha}}{r_\alpha}\,.$$

Since e^{-ikr_α} varies more rapidly with r_α than does $1/r_\alpha$, we may thus write $E_\alpha(P_A)$ approximately as

$$E_\alpha(P_A) \approx \frac{a_\alpha}{R_0^2}\; e^{i(\omega t - 2k r_\alpha + \phi_\alpha)}\,.$$

*For convenience we use a complex (phasor) notation for variables whenever there is no loss of generality.

UNCLASSIFIED

Hence, summing the returns from all scatterers within the antenna beamwidth, we may write the received voltage in Eq. (2) as

$$v_r(t) = \sum_\alpha A_\alpha e^{i(\omega t - 2kr_\alpha + \phi_\alpha)} \quad , \tag{7a}$$

where $A_\alpha \propto a_\alpha / R_0{}^2$. By Eqs. (5) and (2) we thus have

$$v_s = \frac{\sum_\alpha A_\alpha e^{-i(2kr_\alpha - \phi_\alpha)}}{|v_r|} \quad , \tag{7b}$$

where

$$|v_r|^2 \equiv v_r v_r{}^* = \sum_{\alpha=\alpha_{\min}}^{\alpha_{\max}} \left(A_\alpha{}^2 + 2 \sum_{\alpha'>\alpha} A_\alpha A_{\alpha'} \cos \Delta\psi_\alpha \right) , \tag{7c}$$

in which

$$\Delta\psi_\alpha = 2k(r_\alpha - r_{\alpha'}) + \phi_\alpha - \phi_{\alpha'} \ .$$

Substituting Eq. (6b) into the above, we find

$$v_s(t) = \frac{\sum_{\alpha=\alpha_{\min}}^{\alpha_{\max}} A_\alpha e^{-i[\Omega^2 (t-t_\alpha)^2 + \Phi_\alpha]}}{|v_r|} , \tag{8}$$

where

$$\Omega^2 = \frac{kv^2}{R_0}$$

and

$$\Phi_\alpha = \phi_\alpha + 2kR_0 \ .$$

Since the radar beam illuminates changing sets of scatterers as the aircraft travels along the x direction, the summation limits $\alpha_{\min}$ and $\alpha_{\max}$ will be allowed to vary with time. If the scatterers are equally spaced, we require that $M \approx \alpha_{\max} - \alpha_{\min}$ defines a fixed number of scatterers within the antenna beamwidth.

Generation of the Signal Film and Optical Processing

The signal voltage $v_s(t)$ of Eq. (8) is in turn recorded as density variations on optical film in preparation for the optical processor [9]. As the aircraft receives the temporal development of $v_s(t)$, a corresponding amplitude-modulated density trace is deposited on photographic film. This recording of $v_s(t)$ generates the so-called signal film, which is a transparency with an oscillatory grating pattern proportional to $v_s = \cos \Phi$. The optical processor generates a Fresnel diffraction pattern [10] of the signal film grating to produce an image map of the original surface scatterers. We may describe the Fresnel diffraction pattern $m(x)$ by the following convolution of $v_s(t)$ with the transmittance function $h(x)$ of an optical cylindrical lens [9, 11]:

$$m(\tau) = \left| \int_{-T/2}^{T/2} v_s(\tau - \tau')h(\tau')\, d\tau' \right| , \tag{9}$$

where

$$h(\tau) = e^{i\Omega^2\tau^2}$$

and T is the duration of doppler phase history.*

In our point-scatterer formulation the map function is found by substituting Eq. (8) into Eq. (9):

$$m(\tau) = \left| \sum_{\alpha=\alpha_{\min}}^{\alpha_{\max}} e^{-\Omega^2(\tau-t_\alpha)^2} \int_{-T/2}^{T/2} \frac{A_\alpha e^{i[2\Omega^2(\tau-t_\alpha)\tau'-\Phi_\alpha]}}{|v_r(\tau - \tau')|}\, d\tau' \right| , \tag{10}$$

where

$$v_r(\tau) = \left| \sum_{\alpha=\alpha_{\min}}^{\alpha_{\max}} A_\alpha e^{-i[\Omega^2(\tau-t_\alpha)^2+\Phi_\alpha]} \right| .$$

If hard-limiting is omitted, we obtain a corresponding map function for linear synthetic aperture radar:

$$[m(\tau)]_{\text{linear}} = \left| \sum_{\alpha=\alpha_{\min}}^{\alpha_{\max}} e^{-i\Omega^2(\tau-t_\alpha)^2} \int_{-T/2}^{T/2} A_\alpha e^{i[2\Omega^2(\tau-t_\alpha)\tau'-\Phi_\alpha]}\, d\tau' \right| . \tag{11}$$

*In terms of lens optics, T would correspond to the size of the lens aperture.

UNCLASSIFIED

Thus, if A_α and Φ_α are constant in T',

$$[m(\tau)]_{\text{linear}} = T \left| \sum_{\alpha=\alpha_{\min}}^{\alpha_{\max}} A_\alpha e^{-i[\Omega^2(\tau-t_\alpha)^2+\Phi_\alpha]} \frac{\sin \Omega^2(\tau - t_\alpha)T}{\Omega^2(\tau - t_\alpha)T} \right| .$$

Hence in linear processing we resolve each point scatterer at $\tau = t_\alpha$ as $[\sin \Omega^2(\tau - t_\alpha)T] / [\Omega^2(\tau - t_\alpha)T]$. The width $\Delta\tau = 2\pi/\Omega^2 T$ of the main lobe for this function may be interpreted as the minimum resolvable scale size for our radar system. We thus see that larger T (or longer doppler phase histories in the returned signal) improves the radar resolution. The value of $[m(\tau')]_{\text{linear}}$ at each target center also increases in proportion to T.

When A_α or Φ_α are taken as functions of time, or when hard-limiting is employed, one cannot readily evaluate $m(\tau)$ in Eq. (10). In subsequent analysis we shall discuss how fluctuations of Φ_α and nonlinear properties of hard-limiting affect the resolution capabilities of $m(\tau)$.

EVALUATION OF THE MAP FUNCTION

Effect of Random Phase Fluctuations

If the scatterers are assumed to have equal, but random, phase angles $\Phi_\alpha = \tilde{\Phi}_0$, $\alpha = i, 2, \ldots$, Eq. (7b) then shows that $|v_r|$ is independent of $\tilde{\Phi}_0$. Since $\tilde{\Phi}_0$ is assumed to be a stochastic variable, we may interpret the concomitant stochastic map function by ensemble-averaging Eq. (10). We may thus write the ensemble average of the random function $\tilde{m}(\tau)$ in Eq. (10) approximately as*

$$< \tilde{m}(\tau) > = \left| \sum_\alpha e^{-i\,\Omega^2(\tau-t_m)^2} \int_{-T/2}^{T/2} \frac{A_\alpha e^{i2\Omega^2(\tau-t_\alpha)\tau'}}{|v_r(\tau - \tau')|} < e^{-i\tilde{\Phi}_0} > d\tau' \right| .$$

If $< e^{-i\tilde{\Phi}_0} >$ is independent of τ, we may rewrite the above as

$$< \tilde{m}(\tau) > = \left| < e^{-i\tilde{\Phi}_0} > \sum_\alpha e^{-i\Omega^2(\tau-t_\alpha)^2} \int_{-T/2}^{T/2} \frac{A_\alpha e^{i2\Omega^2(\tau-t_\alpha)\tau'}}{|v_r(\tau - \tau')|} d\tau' \right|$$

$$\equiv \left| < e^{-i\tilde{\Phi}_0} > \right| [m(\tau)]_{\Phi_{\alpha=0}} . \tag{12a}$$

*The tilde will be used whenever $m(t)$ has a random component, and $< >$ will denote the associated ensemble average.

Thus the effect of random phase fluctuations is to reduce the deterministic map function $m(\tau)|_{\Phi_{\alpha=0}}$ by the factor $|< e^{-i\Phi_0} >|$. By the ergodic hypothesis we may evaluate this factor as

$$< e^{i\tilde{\Phi}_0} > = \int_{-\Delta}^{\Delta} e^{i\Phi_0} P(\Phi_0)\, d\Phi_0,$$

where Δ is the maximum excursion of $\tilde{\Phi}_0$ and $P(\Phi_0)$ is the probability density function for Φ_0. If $\tilde{\Phi}_0$ is uniformly distributed in the interval $(-\Delta, \Delta)$, we have $P(\Phi_0) = 1/2\Delta$ and

$$< e^{i\tilde{\Phi}_0} > = \frac{1}{2\Delta} \int_{-\Delta}^{\Delta} e^{i\Phi_0} d\Phi_0 = \frac{\sin \Delta}{\Delta} .$$

Thus Eq. (12a) becomes

$$< \tilde{m}(\tau) > = \frac{\sin \Delta}{\Delta} \Big| m(\tau)_{\ \Phi_{\alpha=0}} . \tag{12b}$$

Eq. (12b) shows that increasing phase excursions Δ will reduce the intensity of $< \tilde{m}(\tau) > = 0$. Specifically, in a completely random situation with $\Delta = \pi$, we find that $< \tilde{m}(\tau) > = 0$. This condition illustrates that it is not possible to resolve scatterers with large phase fluctuations.

Having thus obtained a measure of the effect of random phase fluctuations on resolution, we must now evaluate $m(\tau)|_{\Phi_{\alpha=0}}$ by considering hard-limiting aspects of the problem.

Resolution of Weak Targets in the Presence of a Strong Target

If we assume that one scatterer, say $\alpha = 1$, is much stronger than the other scatterers, that is, $A_1 >> A_\alpha$, $\alpha = 2, 3, \ldots$, then Eq. (7c) may be expressed as

$$|v_r(\tau)| \approx A_1 \sqrt{1 + 2 \sum_{\alpha>1} \frac{A_\alpha}{A_1} \cos\, [\Omega^2(\tau_1 - \tau_\alpha)(\tau_1 + \tau_\alpha - 2\tau) + \Phi_1 - \Phi_\alpha]}$$

Hence

$$v_r(\tau)^{-1} \approx \frac{1}{A_1} \left\{ 1 - \sum_{\alpha>1} \frac{A_\alpha}{A_1} \cos\, [\Omega^2(\tau_1 - \tau_\alpha)(\tau_1 + \tau_\alpha - 2\tau) + \Phi_1 - \Phi_\alpha] \right\}.$$

UNCLASSIFIED

Thus Eq. (10) becomes

$$m(\tau) = \left| \sum_{\alpha} e^{-i\Omega^2(\tau-\tau_\alpha)^2} \int_{-T/2}^{T/2} \frac{A_\alpha}{A_1} \left\{ 1 - \sum_{\alpha'>1} \frac{A_{\alpha'}}{A_1} \cos\left[\Omega^2(\tau_1 - \tau_{\alpha'})(\tau_1 + \tau_{\alpha'} - 2\tau + 2\tau') \right.\right.\right.$$

$$\left.\left.\left. + \Phi_1 - \Phi_{\alpha'}\right]\right\} e^{i[2\Omega^2(\tau-\tau_\alpha)\tau' - \Phi_\alpha]}\, d\tau' \right| .$$

This may be expressed as

$$m(\tau) = \left| \sum_{\alpha} \frac{A_\alpha}{A_1} e^{-i\Omega^2(\tau-\tau_\alpha)^2} \int_{-T/2}^{T/2} d\tau' \left\{ e^{i[2\Omega^2(\tau-\tau_\alpha)\tau' - \Phi_\alpha]} \right.\right.$$

$$- \frac{1}{2} \sum_{\alpha'>1} \frac{A_{\alpha'}}{A_1} e^{-i\Omega^2[\tau_1^2 - \tau_{\alpha'}^2 - 2\tau(\tau_1 - \tau_{\alpha'})]} e^{-i(\Phi_\alpha - \Phi_{\alpha'} + \Phi_1)} e^{2i\Omega^2\tau'(\tau - \tau_\alpha + \tau_{\alpha'} - \tau_1)}$$

$$\left.\left. - \frac{1}{2} \sum_{\alpha'>1} \frac{A_{\alpha'}}{A_1} e^{i\Omega^2[\tau_1^2 - \tau_{\alpha'}^2 - 2\tau(\tau_1 - \tau_{\alpha'})]} e^{-i(\Phi_\alpha + \Phi_{\alpha'} - \Phi_1)} e^{2i\Omega^2\tau'(\tau - \tau_\alpha - \tau_{\alpha'} + \tau_1)} \right\}\right| \tag{13}$$

or

$$m(\tau) = \left| e^{-i\Omega^2(\tau-\tau_1)^2} \int_{-T/2}^{T/2} d\tau' \left[1 - \frac{1}{2} \sum_{\alpha>1} \left(\frac{A_\alpha}{A_1} \right)^2 \right] e^{-i\Phi_1} e^{2i\Omega^2(\tau-\tau_1)\tau'} \right.$$

$$+ \frac{1}{2} \sum_{\alpha>1} \frac{A_\alpha}{A_1} e^{-i\Omega^2(\tau-\tau_\alpha)^2} \int_{-T/2}^{T/2} d\tau' e^{-i\Phi_a} e^{2i\Omega^2(\tau-\tau_\alpha)\tau'}$$

$$- \frac{1}{2} \sum_{\alpha} \sum_{\substack{\alpha'>1 \\ \neq\alpha}} \frac{A_\alpha A_{\alpha'}}{A_1^2} e^{-i\Omega^2[(\tau-\tau_\alpha)^2 - (\tau-\tau_{\alpha'})^2 + (\tau-\tau_1)^2]}$$

$$\left. \times \int_{-T/2}^{T/2} d\tau' e^{-i(\Phi_\alpha - \Phi_{\alpha'} + \Phi_1)} e^{2i\Omega^2(\tau - \tau_\alpha + \tau_{\alpha'} - \tau_1)\tau'} \right| \tag{14}$$

$$- \frac{1}{2} \sum_{\alpha>1} \sum_{\alpha'>1} \frac{A_\alpha A_{\alpha'}}{A_1^2} e^{-i\Omega^2[(\tau-\tau_\alpha)^2+(\tau-\tau_{\alpha'})^2-(\tau-\tau_1)^2]}$$

$$\times \int_{-T/2}^{T/2} d\tau' e^{-i(\Phi_\alpha+\Phi_{\alpha'}-\Phi_1)} e^{2i\Omega^2(\tau-\tau_\alpha-\tau_{\alpha'}+\tau_1)} \Bigg| . \qquad \text{(14) Continued.}$$

To interpret this equation, we must consider specific cases of scatterer spacing and phase functions Φ_α. Assuming random phase fluctuations as in Eq. (12a) (the random variable $\widetilde{\Phi}_\alpha$ is uniformly distributed in the interval from $-\Delta_\alpha$ to Δ_α), we may ensemble-average Eq. (14) to obtain

$$< \widetilde{m}(\tau) > = | m_1(\tau) + m_2(\tau) + m_3(\tau) + m_4(\tau) | , \qquad (15)$$

where

$$m_1 = TF_1 \frac{\sin \mu_1}{\mu_1} \left[1 - \frac{1}{2} \sum_{\alpha>1} \left(\frac{A_\alpha}{A_1} \right)^2 \right] e^{-i\mu_1/T} ,$$

$$m_2 = \frac{1}{2} T \sum_{\alpha>1} \frac{A_\alpha}{A_1} F_\alpha \frac{\sin \mu_\alpha}{\mu_\alpha} e^{-i\mu_\alpha/T} ,$$

$$m_3 = - \frac{1}{2} T \sum_{\alpha} \sum_{\substack{\alpha'>1 \\ \neq\alpha}} \frac{A_\alpha A_{\alpha'}}{A_1^2} G_{\alpha\alpha'} \frac{\sin \nu_\alpha}{\nu_\alpha} e^{-i\Omega^2[(\tau-\tau_\alpha)^2-(\tau-\tau_{\alpha'})^2+(\tau-\tau_1)^2]} ,$$

$$m_4 = - \frac{1}{2} T \sum_{\alpha>1} \sum_{\alpha'>1} \frac{A_\alpha A_{\alpha'}}{A_1^2} G_{\alpha\alpha'} \frac{\sin \xi_\alpha}{\xi_\alpha} e^{-i\Omega^2[(\tau-\tau_\alpha)^2+(\tau-\tau_{\alpha'})^2-(\tau-\tau_1)^2]} ,$$

in which

$$F_\alpha = < e^{-i\widetilde{\Phi}_\alpha} >, \quad G_{\alpha\alpha'} = < e^{-i(\widetilde{\Phi}_\alpha - \widetilde{\Phi}_{\alpha'} + \widetilde{\Phi}_1)} >,$$

$$\mu_\alpha = \Omega^2 T(\tau - \tau_\alpha), \quad \nu_\alpha = \Omega^2 T(\tau - \tau_\alpha - \tau_1 + \tau_{\alpha'}), \quad \xi_\alpha = \Omega^2 T(\tau - \tau_\alpha + \tau_1 - \tau_{\alpha'}) .$$

By Eq. (15) we may associate target images of the map function with certain properties of synthetic aperture radar. We see that the first contribution $m_1(\tau)$ will peak at $\mu_1 = 0$ (or at the position of the first scatterer $\tau = \tau_1$), whence $m(\tau)$ represents the map resolution of the first scatterer. Due to hard-limiting, we find that other scatterers enter into the term $-(1/2)\Sigma_{\alpha>1}(A_\alpha/A_1)^2$ and hence cause a reduction in the linearized value of $m_1(\tau)$. The $m_2(\tau)$ factor is seen to peak at $\mu_\alpha = 0$, corresponding to $\tau = \tau_\alpha$. Hence $m_2(\tau)$ represents the map resolution of weaker targets ($\alpha = 2, 3, \ldots$), other than $a = 1$. However, the amplitude of $m_2(\tau)$ at $\mu_2 = 0$ is reduced to half of its correct value obtained

UNCLASSIFIED

when linear processing is employed. This fact may be deduced by comparing $m(\tau)$ in Eq. (11) with $m_1 + m_2$ in Eq. (15). Thus in hard-limited systems the weak-scatterer amplitudes will appear to be reduced by a factor of 2. Mathematically this reduction is due to contributions from nonlinear interaction terms in Eq. (13). As a result of these interactions false scatterers are created on the image map at locations which coincide with the true scattering centers. By superposing these false scatterers (which turn out to have negative amplitudes) with the true scatterer amplitudes, we arrive at a reduced overall amplitude at the image map. Also, this process is manifest in reduction of the strong scatterer, except that its effect is not as great when only a few weak scatterers are present (implying that $(1/2)\Sigma_{\alpha>1}(A_\alpha/A_1)^2 << 1$.

By inspecting the m_3 and m_4 factors, we find that they produce additional images at $\nu_\alpha = 0 = \xi_\alpha$, corresponding to

$$\tau = \tau_\alpha - \tau_{\alpha'} + \tau_1 \equiv \tau_\nu, \qquad \text{when } \nu_\alpha = 0, \tag{16a}$$

$$\tau = \tau_\alpha + \tau_{\alpha'} - \tau_1 \equiv \tau_\xi, \qquad \text{when } \xi_\alpha = 0. \tag{16b}$$

If the set of position variables τ_α, $\alpha = 1, 2, \ldots$ are not integrally related, we find that τ_ν and τ_ξ will not necessarily coincide with the positions, τ_α of the true scatterers. Thus m_3 and m_4 can produce false images at positions other than the scatterer locations, resulting in possible errors in detection. With exception of the $\alpha = 1$ term in m_3, these errors are of second order in weak-scatterer amplitudes and may be neglected relative to the true images. When the scatterers are equally spaced, the τ_α are then integrally related and Eqs. (16) show that the false images fall at the true-image positions. Hence in this case false images would not be observed; only a small change in true-scatterer amplitudes would occur. These conclusions hold for weak scatterers $\alpha = 2, 3$, etc. such that $A_\alpha << A_1$. As will be shown in the section on computer results, multiple strong scatterers of comparable amplitudes can produce noticeable false images at locations unrelated to Eqs. (16). In this case Eq. (12a) must be evaluated by use of irregular expansions in the scatterer amplitudes.

Special Case of Two Targets

Using Eqs. (12b) and (15), we evaluate the map function for two scatterers ($\alpha = 1, 2$, such that $A_1 >> A_2$) as

$$< \tilde{m}(\tau) > = | m_1(\tau) + m_2(\tau) + m_3(\tau) + m_4(\tau) |, \tag{17}$$

where

$$m_1 = \frac{T \sin \Delta_1 \sin \mu_1}{\Delta_1 \mu_1} \left[1 - \frac{1}{2} \left(\frac{A_2}{A_1} \right)^2 \right] e^{-i\mu_1/T}$$

$$m_2 = \frac{1}{2} T \frac{A_2}{A_1} \frac{\sin \Delta_2 \sin \mu_2}{\Delta_2 \mu_2} e^{-i\mu_2/T},$$

$$m_3 = -\frac{1}{2} T \frac{A_2}{A_1} \frac{\sin \Delta_2}{\Delta_2} \frac{\sin \Delta_1}{\Delta_1} \frac{\sin \nu_1}{\nu_1} e^{-i\Omega^2[2(\tau-\tau_1)^2-(\tau-\tau_2)^2]},$$

$$m_4 = -\frac{1}{2}\, T\left(\frac{A_2}{A_1}\right)^2 \left(\frac{\sin \Delta_2}{\Delta_2}\right)^2 \frac{\sin \xi_2}{\xi_2}\, e^{-i\Omega^2[2(\tau-\tau_2)^2-(\tau-\tau_1)^2]},$$

in which

$$\mu_1 = \Omega^2 T(\tau - \tau_1),\ \mu_2 = \Omega^2 T(\tau - \tau_2),$$

$$\nu_1 = \Omega^2 T(\tau - 2\tau_1 + \tau_2),\ \xi_2 = \Omega^2 T(\tau - 2\tau_2 + \tau_1)$$

Δ_1, Δ_2 are maximum deviations of the phases $\tilde{\Phi}_1, \tilde{\Phi}_2$.

By Eq. (17) we see that false images will be created at $\tau = 2\tau_1 - \tau_2 = \tau_1 - (\tau_2 - \tau_1)$ and $\tau = 2\tau_2 - \tau_1 = \tau_2 + (\tau_2 - \tau_1)$. These images are thus spaced about the true scatterers at $\tau = \tau_1$ and τ_2 by an amount $\Delta\tau = \tau_2 - \tau_1$. The strongest false image is given by m_3 as lying to the left of the $\alpha = 1$ scatterer, and, if $\Delta_1 = 0$, its magnitude is equal to that of the $\alpha = 2$ scatterer. Equation (15) shows that the intensity of the αth scatterer will be reduced by random phase fluctuations according to $(\sin \Delta_\alpha)/\Delta_\alpha$. Thus, if $\alpha = 2$ is a fixed scatterer ($\Delta_2 = 0$) and $\alpha = 1$ is fluctuating with $\Delta_1 = \pi$, we can obtain a situation in which $\alpha = 2$ is visible although the stronger scatterer is invisible. Since m_3 depends on interaction between the $\alpha = 1$ and $\alpha = 2$ scatterers, we find that the associated false image will be reduced by random phase fluctuations according to $(\sin \Delta_1 \sin \Delta_2)/\Delta_1\Delta_2$. The false image given by m_4 at $\tau = \tau_2 + (\tau_2 - \tau_1)$ is due to the self interaction of A_2 and hence is not affected by randomness in the $\alpha = 1$ scatterer.

COMPUTER RESULTS

In this section we shall illustrate numerical evaluation of the map function in Eq. (10). By these numerical evaluations we may verify the approximate results of the section "Formulation of the Model" and can also treat more general cases which cannot readily be solved by approximate means. Graphical results will be illustrated for various collections of scatterers.

Definition of Parameters

With reference to Fig. 2, all relevant parameters of our problem may be defined in terms of the system configuration in the azimuthal plane. The parameter L designates the length of scattering surface illuminated by the antenna at any given time. We represent the scattering surface by a collinear set of point scatterers arranged at a constant spacing d. We consider a maximum of n different scattering amplitudes $A_i (i = 1, 2, \ldots, n)$ and assume that this pattern repeats itself with period Λ/v. This periodicity assumption is imposed for simplicity in resolving scatterers at the extremities of our flight path. The radar antenna is pictured as moving along the azimuthal line at a constant speed v. At fixed time intervals $\Delta\tau$ the radar antenna receives the scattered voltage $v_r(t)$ shown in Eq. (2), and we proceed to process this sampled signal according to Eqs. (5) and (9). Accordingly, in our numerical algorithm we approximate the integral in Eq. (9) as

$$m(\tau) = \left| \sum_{n=-N/2}^{N/2} v_s(\tau - n\Delta\tau) h(n\Delta\tau)\Delta\tau \right|, \tag{18}$$

UNCLASSIFIED

where

$$N = \frac{T}{\Delta\tau}$$

and

$$\tau = m\Delta\tau,$$

with

$$m = -\frac{M}{2}, -\frac{M}{2}+1, \ldots, \frac{M}{2},$$

in which

$$M = \frac{\Lambda}{v\Delta\tau}.$$

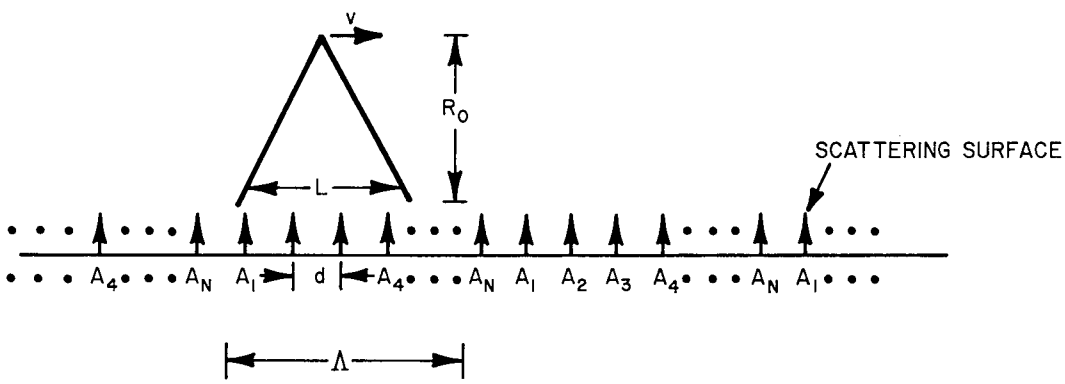

Fig. 2—Configuration corresponding to the relevant parameters:
v = speed of the aircraft along the azimuthal line
$k = 2\pi/\lambda$ = free-space wave number of the radar signal
R_0 = minimum distance from the aircraft to the azimuthal line being mapped
$L \equiv Tv$ = azimuthal length of the antenna illumination
$\Omega^2 L \equiv kvL/R_0$ = highest temporal frequency of the doppler return signal. By the Nyquist sampling theorem we must sample the radar return signal at intervals $\Delta\tau \leqslant 2(2\pi/\Omega^2 L)$
d = spacing between scatterers
$N = \alpha_{max} - \alpha_{min}$ = number of scatterers per antenna beamwidth
Λ = distance such that Λ/v is the period of the scattering-amplitude pattern
A_n = intensity of the nth scatterer
Φ_n = phase of the nth scatterer appearing in Eq. (8)
Δ_n = maximum random phase excursions of the nth scatterer per Eq. (12b)

For sufficiently small $\Delta\tau$ we note that Eq. (18) will converge to the desired Eq. (9). This convergence may be investigated numerically by decreasing $\Delta\tau$ and recomputing Eq. (18) to check whether a significant change in $m(\tau)$ occurs. This check was conducted for each computed result illustrated in this section. As expected, sufficient accuracy was obtained when $\Delta\tau$ satisfied the Nyquist sampling criterion for the function $\cos \Omega^2\tau$, $\tau \leqslant T$. A listing of the computer program used to compute $v_s(\tau)$ and $m(\tau)$ is included in Appendix A.

In the following paragraphs we shall describe plots of some evaluations of Eq. (18) for various amplitudes A_n, phases Φ_n, and scatterer spacings d.

Single Target Per Antenna Beamwidth

In Fig. 3 we plot $m(\tau)$ in Eq. (18) for various values Δ_1 of maximum random phase excursions of Φ_1. A constant amplitude $A_1 = 1$ was chosen, so that v_r of Eq. (7b) is unity. In this case we may simply evaluate Eq. (12a) by using Eq. (11) for $m(\tau)|_{\Phi_1=0}$. We thus find that a single scatterer gives

$$< \tilde{m}(\tau) > = T \left| \frac{\sin \Omega^2(\tau - \tau_1)}{\Omega^2(\tau - \tau_1)T} < e^{-i\Phi_1} > \right| . \tag{19}$$

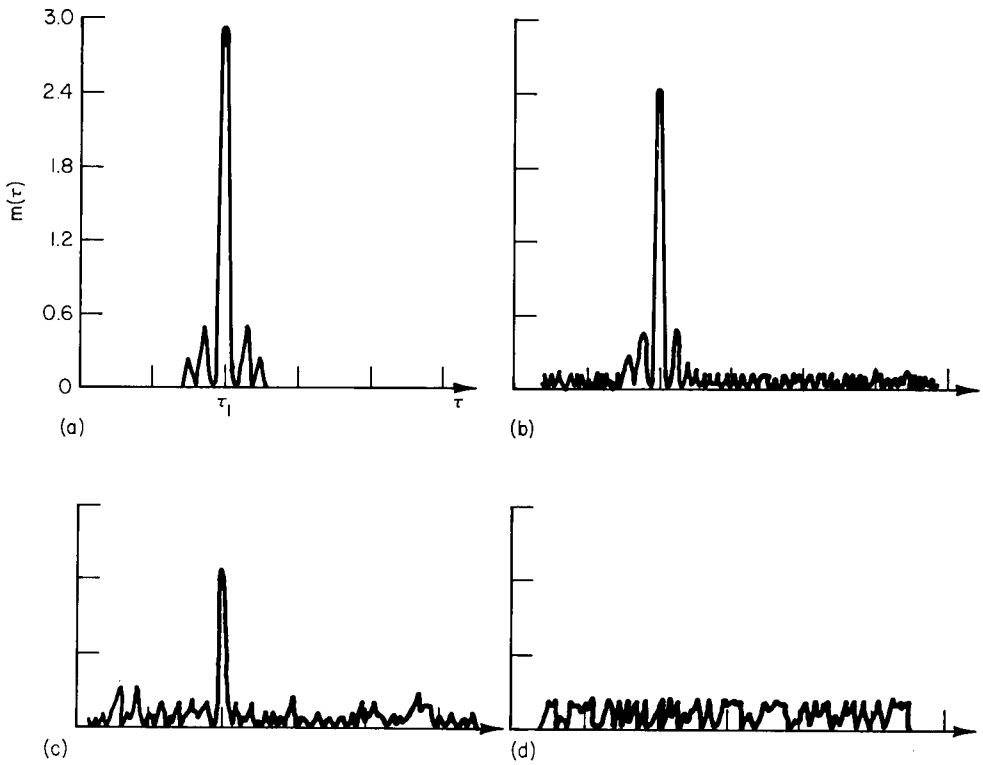

Fig. 3—Numerical evaluation of the map function given by Eq. (10) for $N = \alpha_{max} - \alpha_{min} = 1$, $A_1 = 1$, $L = d = \Lambda = 300$, $R_0 = 5000$, $v = 100$, $k = 20\pi$, $\Omega^2 L/4\pi = 30$, and $\Delta\tau = 3/400$: (a) $\Delta_1 = 0$, (b) $\Delta_1 = \pi/3$, (c) $\Delta_1 = 2\pi/3$, and (d) $\Delta_1 = \pi$

By numerically evaluating Eq. (18), we are able to see the effect of Δ_1 on the ensemble average $< e^{-i\tilde{\Phi}_1} >$. This experiment verified the ergodic assumption used in deriving Eq. (12b).

Figure 3a plots $m(\tau)$ for the deterministic case $\Delta_1 = 0$.* We see that the amplitude of $m(\tau_1)$ corresponds to the assumed value $T = 3$, and its width corresponds to $2\pi/\Omega^2 T$,

*Since our primary concern is to illustrate the amplitude of the map positions at each scatterer center with as much simplicity as possible, we draw only the main lobes of $m(\tau)$ at each scatterer center $\tau - \tau_\alpha$ and omit drawing that portion of $m(\tau)$ due to side-lobe variation. Thus only the main lobe of Eq. (19) can be compared with Fig. 3. This simplified method of presenting the numerical results is also used in Figs. 4 through 9.

UNCLASSIFIED

thus verifying the equivalence of Eqs. (18) and (19). In Figs. 3b through 3d we plot $m(\tau)$ for $\Delta_1 = \pi/3$, $2\pi/3$, and π respectively. These figures illustrate how the level of $m(\tau)$ decreases according to $(\sin \Delta_1)/\Delta_1$ as Δ_1 is increased. In a completely random case ($\Delta_1 = \pi$) we find that Eq. (18) reduces to a low-amplitude rapidly fluctuating function in such a manner that we are no longer able to resolve the scatterer. The results agree very well with Eq. (12b) at $\tau = \tau_1$. At other points $\tau \neq \tau_1$, we find that the level of rapid fluctuations increases with Δ_1, in accord with the increased randomness in target position. Since these rapid fluctuations are sensitive to the random sequence of values chosen for Φ_1, we note that their ensemble average would be zero.

We may interpret randomness of phase $\widetilde{\Phi}_1$ in another manner. By Eq. (8), we find that a change of Φ_α is equivalent to a change in $(\tau - \tau_\alpha)$, corresponding (for given τ) to a change in the scatterer position τ_α. Hence a random $\widetilde{\Phi}_\alpha$ implies a random fluctuation in the position of the αth scatterer. Under such changing scatterer positions it is understandable that random phase hampers one's ability to resolve the scattering center.

Two Targets Per Antenna Beamwidth

Figure 4 illustrates resolution of two scatterers. To conform with the approximate treatment used in Eq. (13) we assume $A_2 = A_1/4$. Figure 4a shows $m(\tau)$ in the absence of hard-limiting. To calculate this case, we substitute $|v_r| = 1$ in Eq. (8) and insert the so-computed $v_s(t)$ into Eq. (18) to obtain the unlimited (or linearized) map function of Fig. 4a. In this manner we are able to resolve the target locations unaffected by other corrupting factors and can thus provide a reference for comparing effects of hard-limiting and random phase fluctuations. We note that Fig. 4a corresponds to Eq. (11) for $\alpha_{max} - \alpha_{min} = 2$.

In Fig. 4b we plot Eq. (18) when hard-limiting is employed for the deterministic case $\Delta_\alpha = 0$. We find that the two scatterers are resolved at $\tau = \tau_1$ and τ_2 according to Eq. (17). As expected, the relative amplitude of A_2 at $\tau = \tau_2$ appears as half of its true value and, as predicted by m_3 and m_4 in Eq. (15), we also find false images at $\tau = \tau_1 - (\tau_2 - \tau_1)$ and $\tau = \tau_2 + (\tau_2 - \tau_1)$. Figure 4c shows $m(\tau)$ when not only hard-limiting is assumed but random phase excursions $\Delta_1 = \Delta_2 = \pi/3$ are assumed. As predicted by Eq. (17) the effect of random phase is to reduce the scatterer amplitude at $\tau = \tau_1$ and τ_2 by the factor $(3/2\pi) \sin (2\pi/3)$ and the ghost images are reduced by $(3/2\pi)^2 \sin^2(2\pi/3)$. There is also a slight increase of background small-scale fluctuations in $m(\tau)$ at points $\tau \neq \tau_1$ and τ_2 due to randomness in the scatterer positions.

Figure 4d shows $m(\tau)$ without hard-limiting with $\Delta_1 = \pi$ and $\Delta_2 = 0$. This case corresponds to a fixed scatterer ($\alpha = 2$) near a randomly moving strong scatterer ($\alpha = 1$), and as expected we find that the $\alpha = 2$ scatterer is mapped as in Fig. 4a but the $\alpha = 1$ scatterer cannot be resolved; only a low-level random fluctuation is imaged at $\tau = \tau_1$. In Fig. 4e we show $m(\tau)$ under the same random phase condition, but with hard-limiting employed. As shown by Eq. (17), we then find that the scatterer resolution at $\tau = \tau_2$ is reduced by half. However the $\alpha = 1$ scatterer and false scatterers do not appear due to the fact that $\Delta_1 = \pi$. When we also assume randomness in Φ_2 (namely $\Delta_1 = \Delta_2 = \pi$), we obtain a completely random case and do not find any discernable image. This is illustrated in Fig. 4f for the hard-limited case, where only a low-level background fluctuation is mapped.

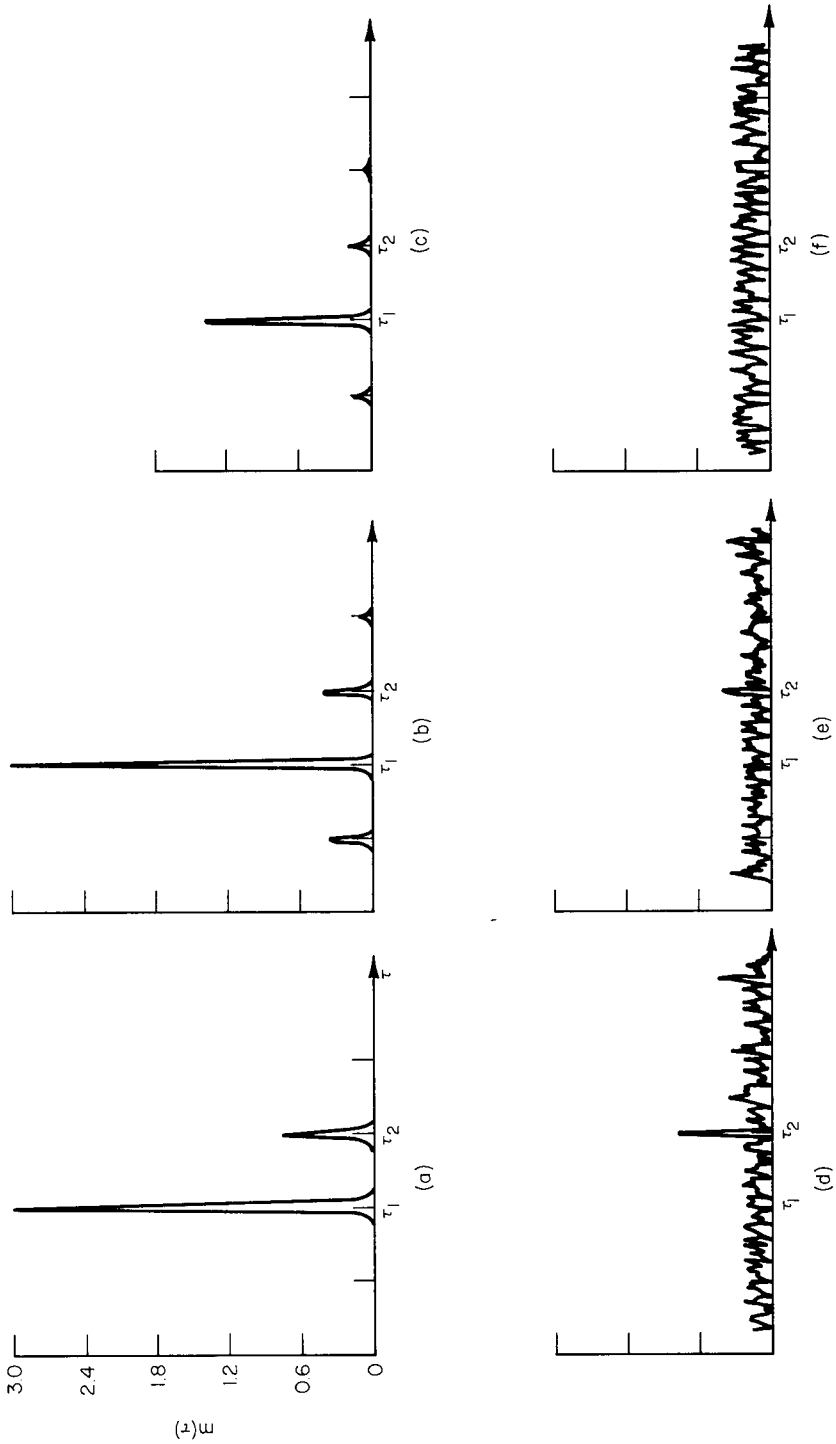

Fig. 4—Numerical evaluation of the map function given by Eq. (10) for two targets at $\tau = \tau_1$ and τ_2 with $A_1 = 1$, $A_2 = 0.25$, $d = 30$, $L = \Lambda = 300$, $R_0 = 5000$, $v = 100$, $k = 20\pi$, $\Omega^2 L/4\pi = 30$, and $\Delta\tau = 3/400$; (a) Unlimited; $\Delta_1 = \Delta_2 = 0$, (b) Hard-limited; $\Delta_1 = \Delta_2 = 0$, (c) Hard-limited; $\Delta_1 = \Delta_2 = 2\pi/3$, (d) Unlimited; $\Delta_1 = \pi$, $\Delta_2 = 0$, (e) Hard-limited; $\Delta_1 = \pi$, $\Delta_2 = 0$, and (f) Hard-limited; $\Delta_1 = \Delta_2 = \pi$

UNCLASSIFIED

Three Targets Per Antenna Beamwidth

Figure 5 illustrates the effect of hard-limiting in resolution of two weak targets in the presence of a strong target. The deterministic case $\Delta_\alpha = 0$, $\alpha = 1, 2, 3$, is considered. Figures 5a and 5c show the unlimited $m(\tau)$ for two different target spacings. The corresponding hard-limited $m(\tau)$ for these two cases is shown in Figs. 5b and 5d respectively. In going from Fig. 5a to Fig. 5b, we see that two symmetrically spaced weak signals produce a symmetrical arrangement of false images. We note that the relative amplitudes of A_2 and A_3 in Fig. 5b are slightly larger than predicted by m_2 in Eq. (15). This enhancement is due to reinforcement by false images which also occur at $\tau = \tau_2$ and τ_3. In Fig. 5d we see that an unsymmetrical assortment of scatterers will produce a different distribution of false images. The largest false image is due to interaction between the two closest scatterers and occurs analogous to the two-scatterer case of Fig. 4b. All other false images are seen to be second-order interactions.

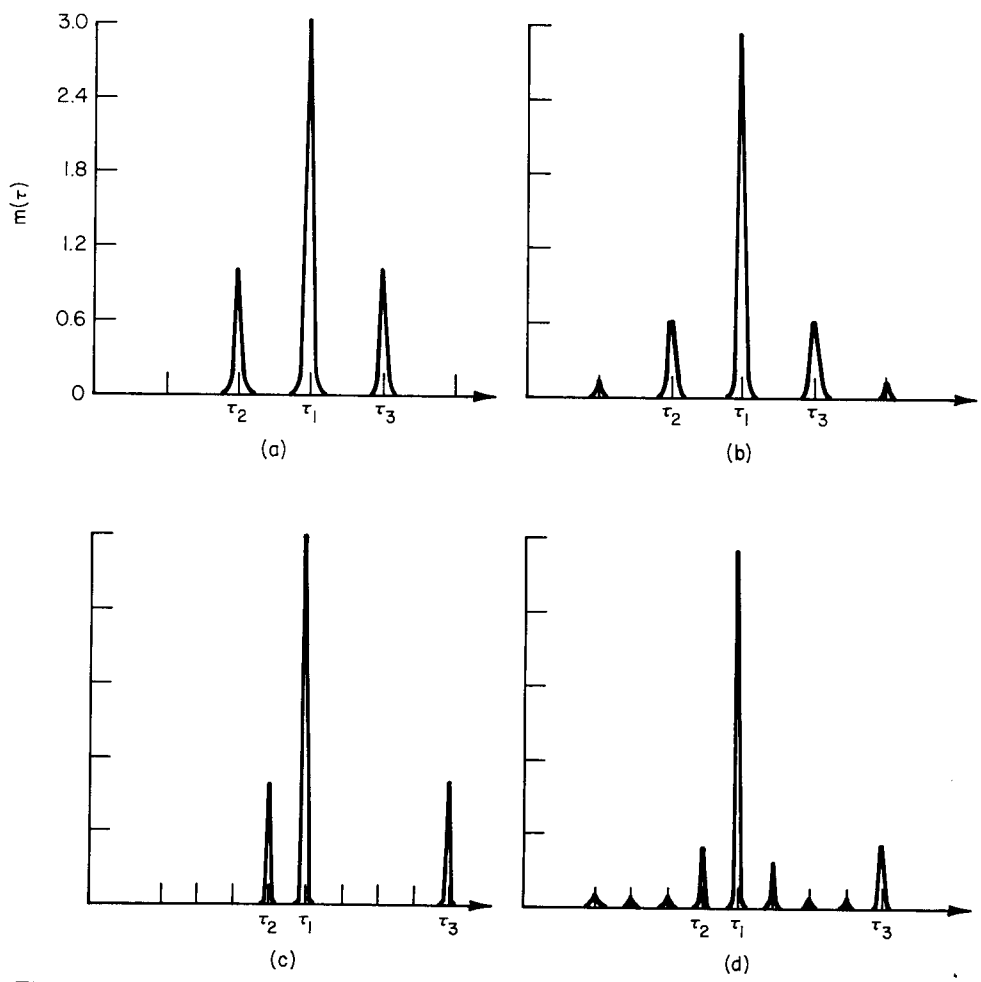

Fig. 5—Map function for three targets at $\tau = \tau_1$, τ_2, and τ_3 with $A_1 = 1$, $A_2 = A_3 = 0.3$, $d = 30$, $L = \Lambda = 300$, $R_0 = 5000$, $v = 100$, $k = 20\pi$, $\Omega^2 L/4\pi = 30$, $\Delta\tau = 3/400$, and $\Delta_1 = \Delta_2 = \Delta_3 = 0$; (a) Unlimited, (b) Hard-limited, (c) Unlimited, and (d) Hard-limited

Figure 6 illustrates the effect of random phase fluctuations, by plotting the resolution of the cases in Figs. 5c and 5d for nonzero Δ_α. In Fig. 6a we plot the unlimited $m(\tau)$ of Fig. 5c, except that we now assume $\Delta_3 = \pi$. As expected, complete randomness of the $\alpha = 3$ scatterer prevents resolution of its scattering center. Figure 6b shows the hard-limited map for the same case. Again we see that the $\alpha = 3$ scatterer cannot be resolved. The only false image appearing is due to the interaction of the deterministic $\alpha = 1$ and $\alpha = 2$ scatterers. The other false images of Fig. 5d do not appear, since they involve interactions among random scatterers and hence are not seen in the averaging process. Also, the relative level of the $\alpha = 2$ scatterer is half of its true level. Thus, except for the low-level random background fluctuations for $\tau \neq \tau_1$, τ_2, or τ_3, this three-scatterer problem yields a map which is very similar to that of the two-scatterer problem. Figures 6c and 6d show $m(\tau)$ for the unlimited and hard-limited cases respectively when $\Delta_1 = \Delta_2 = \pi$ and $\Delta_3 = 0$. In this case, we can resolve only the $\alpha = 3$ scatterer. Although Fig. 6d does not have false images, we nevertheless observe its hard-limited feature in that the amplitude of the $\alpha = 3$ scatterer is only half of its true value. Figures 6e and 6f plot $< \tilde{m}(\tau) >$ for the unlimited and hard-limited cases respectively, assuming $\Delta_\alpha = \pi$, $\alpha = 1, 2, 3$. We find that this condition causes an unresolvable situation, in that $m(\tau)$ has no apparent features at $\tau = \tau_\alpha$, $\alpha = 1, 2, 3$. The random background fluctuations which occur may exhibit peaks which could be mistaken as scatterer images; however we expect that the ensemble average of these fluctuations would be zero.

The results of Fig. 6 are seen to be in close agreement with Eq. (15), since this equation correctly predicts suppression of weak targets and false image generation due to nonlinear interactions, including effects due to random phase variations. However, as the number of scatterers increases, it becomes more difficult to interpret Eq. (15) without the aid of a computer. Subsequent paragraphs describe some numerical experiments involving larger collections of scatterers.

Ten Targets Per Antenna Beamwidth

To show effects of hard-limiting, $m(\tau)$ is plotted in Fig. 7 for various arrangements of deterministic scatterers. Figures 7a and 7b show $m(\tau)$ for ten equally spaced and equal-amplitude scatterers for the unlimited and hard-limited cases respectively. In comparing these two cases, we find that the hard-limited map resolves the individual scatterers quite well but with smaller intensity than those of the unlimited map. In addition hard-limiting causes false images to appear midway between the scatterers. Equation (15) cannot be expected to describe this example, since we do not satisfy the weak-scatterer assumption; hence we prefer to interpret this case on the basis of the computed result.

Figures 7c and 7d plot a case which is describable by Eq. (15). Figure 7c plots the unlimited map function to show the basic arrangement of scatterers. The corresponding hard-limited case is shown in Fig. 7d. In this case we note that false images are no longer present between the scatterers. As predicted by $m_1(\tau)$ in Eq. (15), an effect of nonlinearities in this case is to reduce the amplitude of the strong target, thus resulting in a higher amplitude for the weak targets relative to the strong target. This enhanced relative amplitude for weak scatterers causes the hard-limited map function to appear similar to the unlimited map function. For this reason, a sufficiently high number of weak scatterers is said to linearize a hard-limited map system [4, 12]. In this case, target suppression of weak scatterers will not occur, and one can obtain a fairly accurate measure of

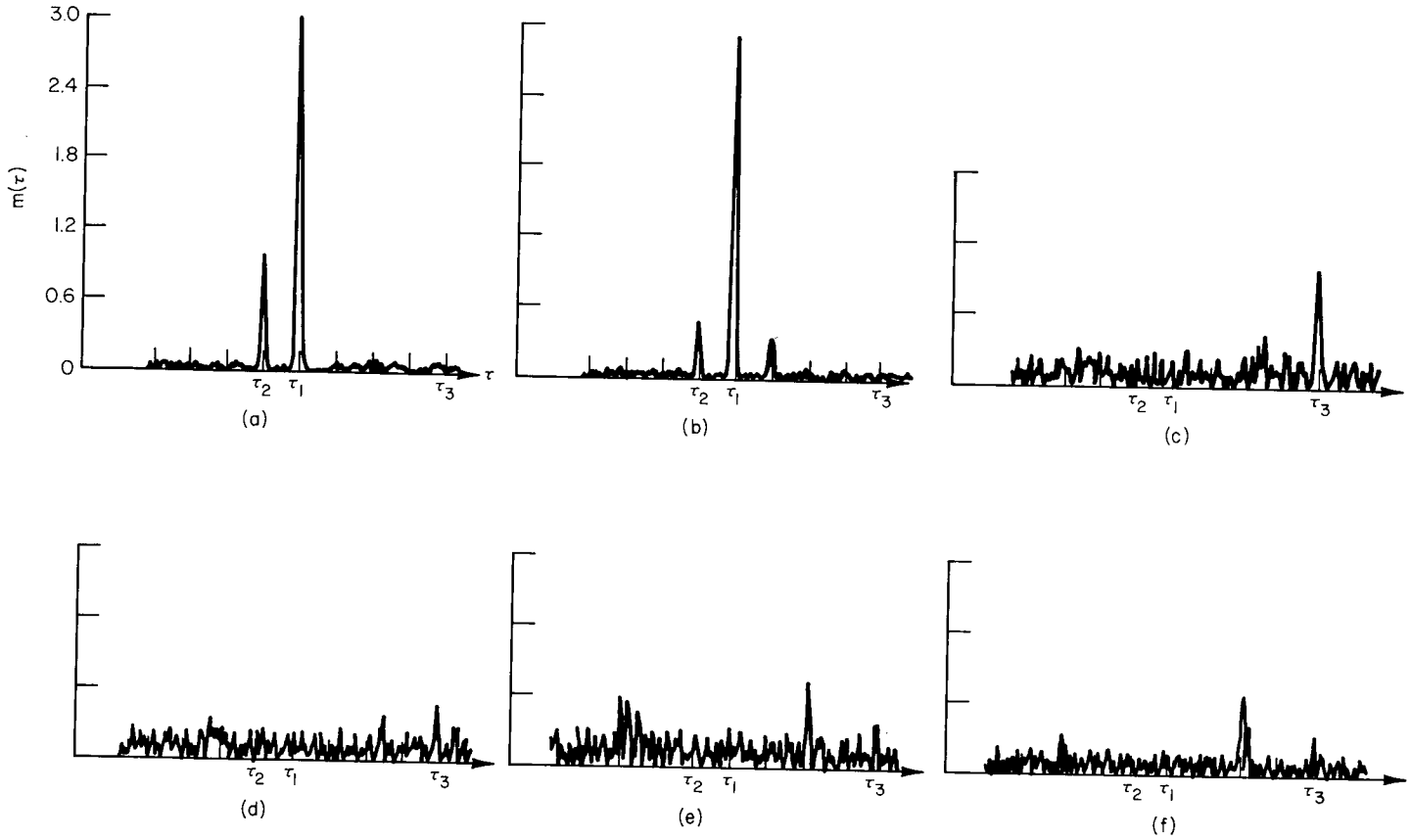

Fig. 6—Map function for three targets at $\tau = \tau_1, \tau_2$, and τ_3 with $A_1 = 1$, $A_2 = A_3 = 0.3$, $d = 30$, $L = \Lambda = 300$, $R_0 = 5000$, $v = 100$, $k = 20\pi$, $\Omega^2 L/4\pi = 30$, and $\Delta\tau = 3/400$: (a) Unlimited; $\Delta_1 = \Delta_2 = 0, \Delta_3 = \pi$, (b) Hard-limited; $\Delta_1 = \Delta_2 = 0, \Delta_3 = \pi$, (c) Unlimited; $\Delta_1 = \Delta_2 = \pi$, $\Delta_3 = 0$, (d) Hard-limited; $\Delta_1 = \Delta_2 = \pi$, $\Delta_3 = 0$, (e) Unlimited; $\Delta_1 = \Delta_2 = \Delta_3 = \pi$. and (f) $\Delta_1 = \Delta_2 = \Delta_3 = \pi$

UNCLASSIFIED

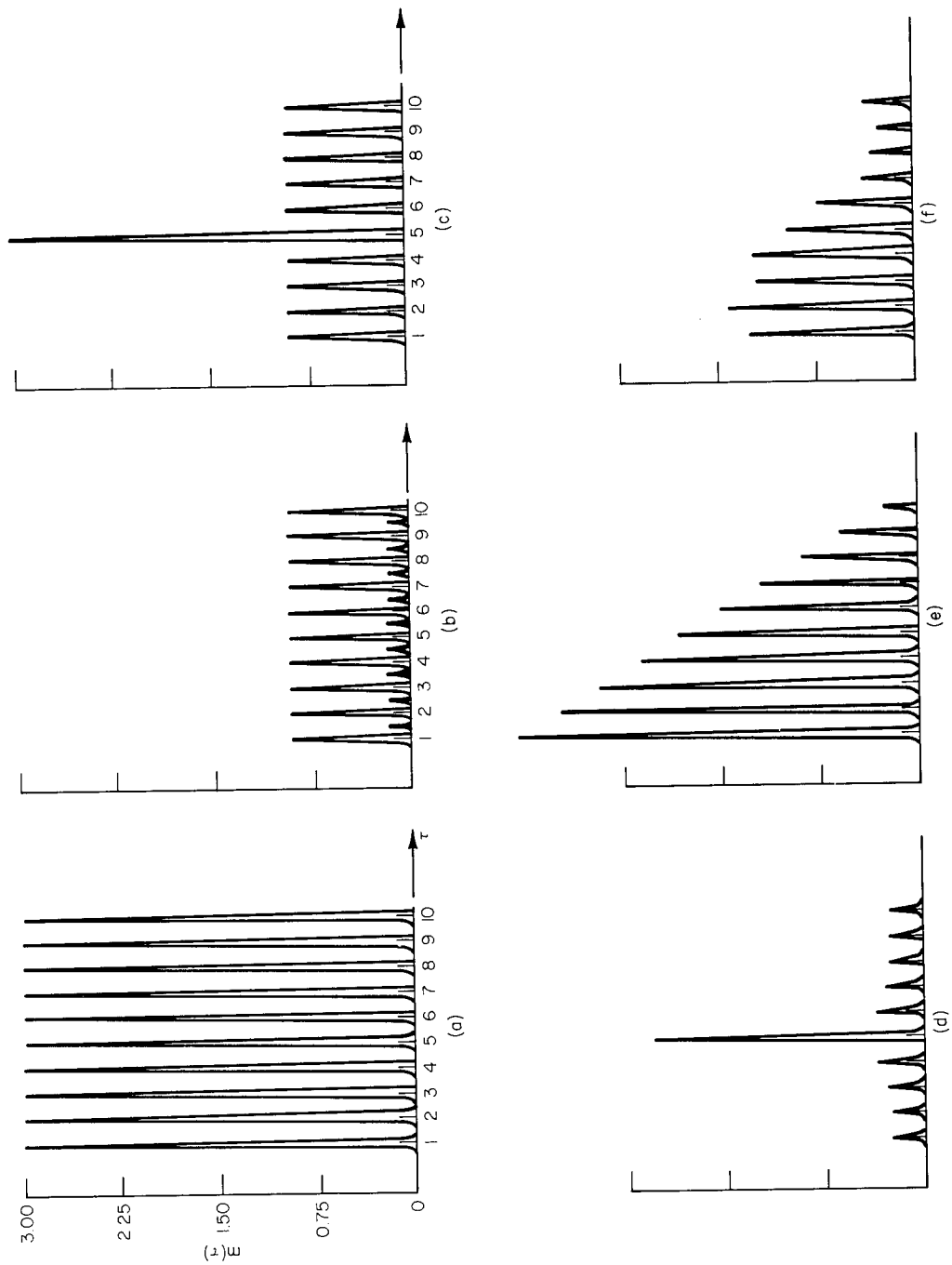

Fig. 7—Map function for ten fixed targets at $\tau = \tau_n$, $n = 1$ through 10, with $d = 30$, $L = \Lambda = 300$, $R_0 = 5000$, $v = 100$, $k = 20\pi$, $\Omega^2 L/4\pi = 30$, $\Delta\tau = 3/400$, and $\Delta_n = 0$, $n = 1$ through 10; (a) Unlimited; $A_n = 1$, $n = 1$ through 10, (b) Hard-limited; $A_n = 1$, $n = 1$ through 10, (c) Unlimited; $A_5 = 1$; $A_n = 0.3$, $n \neq 5$, (d) Hard-limited; $A_5 = 1$; $A_n = 0.3$, $n \neq 5$, (e) Unlimited; $A_n = 1/n$, $n = 1$ through n, and (f) Hard-limited; $A_n = 1/n$, $n = 1$ through 10

UNCLASSIFIED

target strength. By Eq. (15), we note that such a "linearization" can be expected when the term $\Sigma_{\alpha>1}(A_\alpha/A_1)^2$ in m_1 is sufficiently large. (Since we require $A_\alpha << A_1$, $\alpha = 2, 3, \ldots$, it follows that a large number of targets are required.)

To show how hard-limiting may affect one's ability to measure relative target strengths, Figs. 7e and 7f show a case of ten scatterers with linearly decreasing amplitudes. The unlimited case is shown in Fig. 7e. In the hard-limited map of Fig. 7f we observe a peculiar modulation which enhances relative scatterer amplitudes for certain portions of $m(\tau)$ and suppresses them in other regions. The enhancement occurs in the region of strong scatterers, indicating that this effect is due to interaction among strong scatterers. The suppression occurs in the region of weaker scatterers, as is customary in hard-limited signals [4].

Figure 8 plots the resolution of ten scatterers with random phase fluctuations. Figure 8a shows the unlimited $m(\tau)$ when $\Delta_6 = \pi$, and $\Delta_\alpha = 0$, $\alpha \neq 6$. As expected, we find that the $\alpha = 6$ scatterer cannot be resolved. The hard-limited version is shown in Fig. 8b, where we see some interesting suppression effects of adjacent scatterers due to a single random scatterer. False images are found midway between the targets but, due to the $\alpha = 6$ random target, they appear with slightly varying strengths. In Figs. 8c and 8d we assume $\Delta_\alpha = \pi$, $\alpha \neq 6$ or 7, and $\Delta_6 = \Delta_7 = 0$. To establish a reference map for comparison, Fig. 8c shows the unlimited $m(\tau)$. The hard-limited $m(\tau)$ of Fig. 8d shows a very similar resolution of the fixed ($\alpha = 6, 7$) scatterers, with a fairly accurate display of the true relative scatterer strengths. Thus we again find an effective linearization of hard-limited maps of many scatterers with random phase variations. We cannot use Eq. (15) to explain this "linearization," since the A_α, $\alpha \neq 1$, of Figs. 8c and 8d do not satisfy the weak scatterer assumption; so that we must heuristically attribute this phenomena to many-scatter and random-phase effects. To show the dependence of this "linearization" on the amplitude of A_α, $\alpha \neq 1$, Figs. 8e and 8f show $m(\tau)$ for decreasing strengths of the background ($\alpha \neq 1$) scatterers. As expected, we see by Figs. 8d, 8e, and 8f that "linearization" of hard-limited maps requires that the background scatterers be of sufficiently high strength. This follows since background scatterers cause a reduction of m_1 in Eq. (15) through the term $(1/2)\Sigma_{\alpha>1}(A_\alpha/A_1)^2$. Since the ratio m_2/m_1 increases as m_1 is reduced, we thus obtain the effective "linearization" phenomena. Thus we can conclude that "linearization" of hard-limited maps occurs if the background scatterers meet the criterion. Figure 8f shows a case in which $\Sigma_{\alpha>1}(A_\alpha/A_1)^2 < 1$. In this case the background scatterers have little effect on "linearization," and $m(\tau)$ begins to show features of hard-limiting such as false images and image suppression.

Resolving Uniform Arrangements of Many Targets

To simulate some conditions which are encountered in mapping terrain and ocean surface [7], a computer run involving 60 scatterers with a step discontinuity in scattering amplitudes was made. Figure 9a shows the true scatterer arrangement by plotting the unlimited map function.* Of the 60 scatterers, the antenna beamwidth was prescribed to illuminate ten scatterers at any given instant of observation (with reference to Fig. 2, the ratio L/Λ for this case would equal 1/6). The corresponding hard-limited map of this

*For simplicity Fig. 7 shows only the peaks of the main lobes at each scattering center. Thus each of the 60 vertical lines drawn indicates the amplitude of a scattering center.

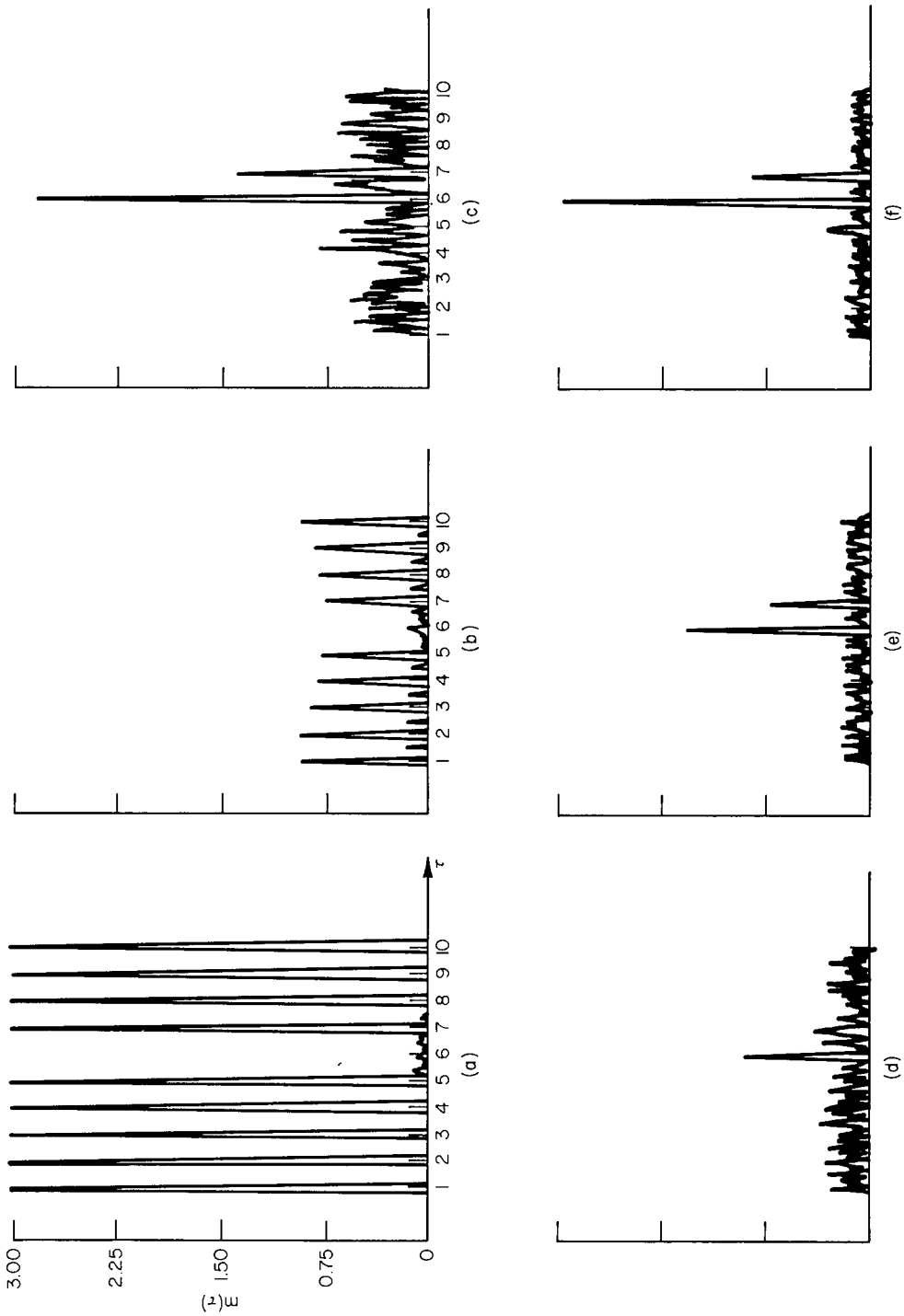

Fig. 8—Map function for ten targets at $\tau = \tau_n$, $n = 1$ through 10, with random phase and with $d = 30$, $L = \Lambda = 300$, $R_0 = 5000$, $v = 100$, $k = 20\pi$, $\Omega^2 L/4\pi = 30$, and $\Delta\tau = 3/400$: (a) Unlimited; $\Delta_6 = \pi$; $\Delta_n = 0$, $n \neq 6$; $A_n = 1$, $n = 1$ through 10, (b) Hard-limited; $\Delta_6 = \pi$; $\Delta_n = 0$, $n \neq 6$; $A_n = 1$, $n = 1$ through 10, (c) Unlimited; $\Delta_n = \pi$, $n \neq 6$ or 7, $\Delta_6 = \Delta_7 = 0$; $A_n = 1$, $n \neq 7$, $A_7 = 0.5$, (d) Hard-limited; $\Delta_n = \pi$, $n \neq 6$ or 7; $\Delta_6 = \Delta_7 = 0$; $A_n = 1$, $n \neq 7$; $A_7 = 0.5$, (e) Hard-limited; $\Delta_n = \pi$, $n \neq 6$ or 7; $\Delta_6 = \Delta_7 = 0$; $A_6 = 1$; $A_n = 0.5$, $n \neq 6$, and (f) Hard-limited; $\Delta_n = \pi$, $n \neq 6$ or 7; $\Delta_6 = \Delta_7 = 0$; $A_6 = 1$; $A_n = 0.5$, $n \neq 6$

UNCLASSIFIED

problem is shown on Fig. 9b. As is evident by comparing $m(\tau)$ away from the discontinuity, the relative scatterer intensities cannot be resolved by hard-limited processing. Thus we see that the intensity of the weak scatterers in the image plane is equal to that of the strong scatterers. However near the discontinuous region we begin to distinguish relative amplitudes of scatterers, and Fig. 9b shows the tendency of $m(\tau)$ to seek proper relative levels in such regions.

Figures 9c and 9d plot $m(\tau)$ for assumed random variation of amplitude and phase respectively. In Fig. 9c the phase Φ_n of each scatterer was held constant and the amplitudes A_n were varied in the random fashion stated in the figure subtitle. Physically this condition represents fixed point-targets with random scattering cross sections. As we see from Fig. 9c, the map function for this case is similar to the deterministic case of Fig. 9b. Thus a fixed succession of targets with a discontinuous change in their scattering cross sections produce hard-limited maps with a characteristic doublet-type oscillation at the point of discontinuity. In Fig. 9d the amplitudes A_n were held fixed and the phases Φ_n were selected randomly. As in Figs. 3, 4, 6, and 8 this case implies a random motion of target positions; hence we cannot resolve the scattering centers. Our inability to resolve the scatterers is evidenced by the random variation in $m(\tau)$ of Fig. 9d.

SUMMARY

A study is made of hard-limited synthetic aperture resolution of point targets. We derive a mathematical representation of our point-scatterer model and synthetic aperture radar system. The corresponding map function is formulated by match-filtering the hard-limited return signal via an optical processor. An approximate evaluation is then made of the map function. In this analysis we include a method of treating random phase variations of the point targets. The hard-limited aspect of our problem is treated approximately by assuming that a single strong scatterer is imbedded in a set of much weaker scatterers. By this method we derive Eq. (15), which isolates causes of image suppression and false image generation due to hard limiting. As an example, the special case of two point-targets is considered in detail.

Finally we consider results on numerical evaluation of the map function. This enables us to treat more general target arrangements which cannot be easily treated by analytical means. Effects of various target arrangements and random phase variations are summarized in graphical form, and some interesting properties such as target resolution in the presence of random variation of background targets and false-image generation due to nonlinear interactions among targets are discussed. Under certain conditions of background targets, we show that hard-limited maps are not appreciably different from unlimited (or linearly processed) maps, in which case the background targets are said to "linearize" the system. Although such a phenomenon has already been predicted [4, 12], we present some different situations in which this occurs and give a simplified explanation of its origin. In an effort to simulate mapping of certain terrain and ocean surfaces, we also present plots of the map function for a set of targets arranged with a discontinuous change in their scattering cross sections. The corresponding map function for this case is characterized by a doublet-type behavior at the point of discontinuity. The computer program is listed in Appendix A.

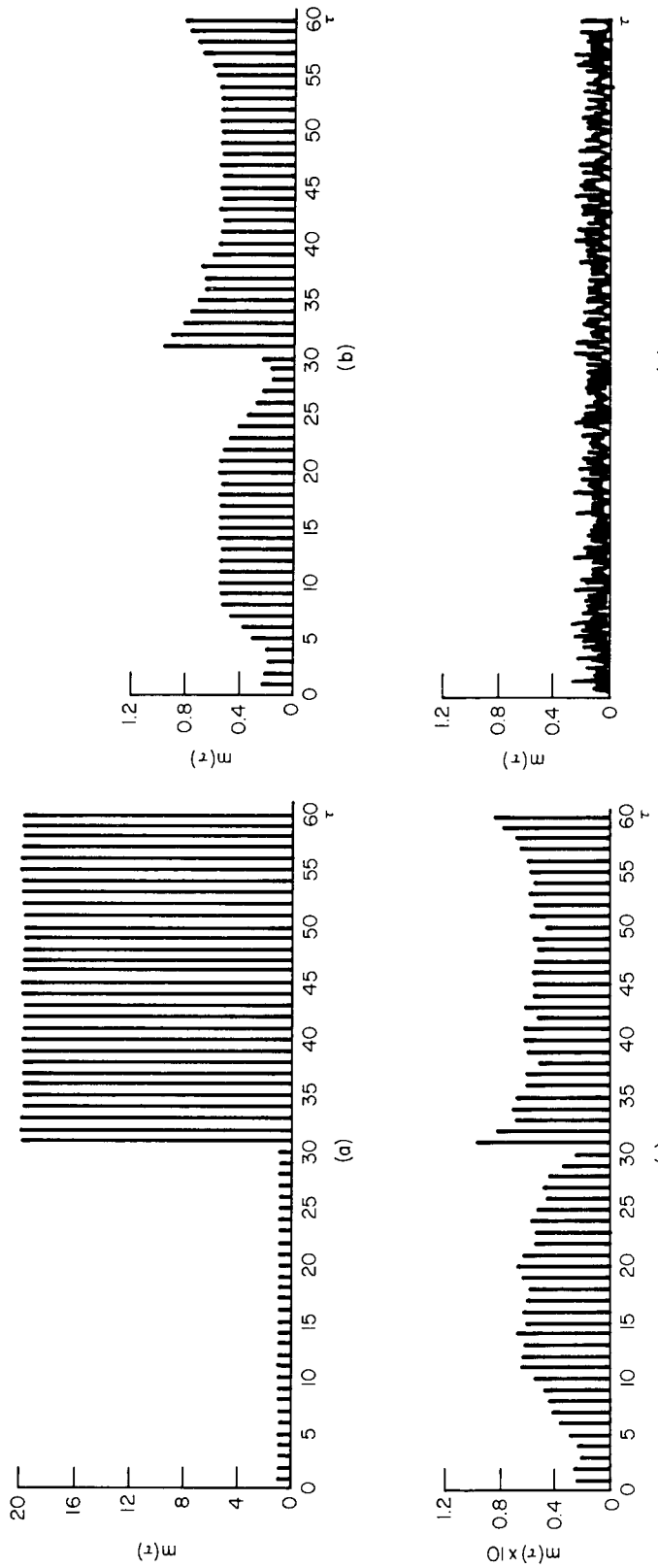

Fig. 9—Map function for 60 targets with a step discontinuity in scattering amplitudes with $d = 20$, $L = 200$, $\Lambda = 1200$, $R_0 = 5000$, $v = 100$, $k = 20\pi$, $\Omega^2 L/4\pi = 20$, and $\Delta\tau = 3/200$: (a) Unlimited; $A_n = 0.5$, $n = 1$ through 30; $A_n = 10$, $n = 31$ through 60; $\Delta_n = 0$, $n = 1$ through 60, (b) Hard-limited; $A_n = 0.5$, $n = 1$ through 30; $A_n = 10$, $n = 31$ through 60; $\Delta_n = 0$, $n = 1$ through 60. Note that the ordinate is expanded by a factor of 10 relative to that of (a), (c) Hard-limited; $A_n = 0.5R_n$, $n = 1$ through 30, and $A_n = 10R_n$, $n = 31$ through 60, where R_n is a random variable uniformly distributed between 0 and 1; $\Delta_n = 0$, $n = 1$ through 60, and (d) Hard-limited; $A_n = 0.5$, $n = 1$ through 30; $A_n = 10$, $n = 31$ through 60; $\Delta_n = \pi$, $n = 1$ through 60

UNCLASSIFIED

ACKNOWLEDGMENTS

The author is indebted to Messrs. N.W. Guinard and M.B. Laing and Dr. G.R. Valenzuela for their encouragement and numerous discussions.

REFERENCES

1. C.W. Sherwin, J.P. Ruina, and R.D. Rawcliffe, "Some Early Developments in Synthetic Aperture Radar Systems," IRE Trans. Mil. Elect. *MIL-6*, 111 (Apr. 1962).
2. W.M. Cady, M.B. Karelitz, and L.A. Turner, editors, "Radar Scanners and Radomes," MIT Rad. Lab. Series, V26, New York, McGraw-Hill, 1948, p 11.
3. R.O. Harger, "Synthetic Aperture Radar Systems, Theory and Design" New York, Academic Press, 1970:
   (a) Chap. VII
   (b) Chap. IV
4. B.D. Steinberg, "Hard Limiting in Synthetic Aperture Signal Processing, Part I, Analysis," report prepared for NRL, Sept. 1972.
5. H.H. Woerrlein, "Capture and Spurious Target Generation Due to Hard Limiting in Large Time-Bandwidth Product Radars," NRL Report 7001, Dec. 1969.
6. J.C. Nolen, "Effects of Limiting on Multiple Signals," Symposium Proceedings, RADC-TR-59-161, Sept. 1959, p. 295.
7. N.W. Guinard, "Radar Detection of Oil Spills," Joint Conf. Sensing of Environment Pollutants, Nov. 8-10, 1971, AIAA paper 71-1072.
8. J.W. Wright, "A New Model for Sea Clutter," IEEE Trans. on Ant. and Prop. *AP-16*, 217 (1968).
9. L.J. Cutrona, E.N. Leith, L.J. Porcello, and W.E. Vivian, "On the Application of Coherent Optical Processing Techniques to Synthetic-Aperture Radar," Proc. IEEE *V54*, 1026 (1966).
10. J.W. Goodman, "Introduction to Fourier Optics," New York, McGraw-Hill, 1968, p. 60.
11. A. Vander Lugt, "Operational Notation for the Analysis and Synthesis of Optical Data-Processing Systems," Proc. IEEE *V54*, 1055 (1966).
12. E.D. Banta, "Far Field Properties of Wide Band Planar Arrays with Nonlinear Processing," IRE International Convention Record, Part I, p. 95, 1961.

Appendix A

Computer Program to Evaluate $v_s(\tau)$ and $m(\tau)$

```
'FTN,L,X
      PROGRAM SUM
      REAL M,MN
C THE DIMENSION OF C,D,CN SHOULD =KL
      COMPLEX C(800),CM(800),CN(800),PI,CPN,CK,CPM,DC
C THE DIMENSION OF M,M1,M2, SHOULD = KM
      DIMENSION D(800),M(800),RC(800),MN(800),RCM(800)
C THE DIMENSION OF A SHOULD =NA
      DIMENSION A(200)
C KL=EVEN NO. OF LOOKS IN TRAVELLING THE OBSERVATION REGION
      KL=400
      NP=1
C KM=NO. OF LOOKS WITHIN ONE ANTENNA BEAM WIDTH
      KM=KL/NP
      NA=10
C NTS SHOULD BE EVEN
      NTS=NA*NP
      NTS2=NTS/2
      DX=30.
C DEFINITION OF AMPLITUDES A
      DO 3 K=1,NTS
    3 A(K)=0.3
      A(5)=1.0
      NA2=NA/2
      SN=NTS
      SN1=KL
      SN=SN/SN1
      VA=100
      R0=5000.
      K0=62.8
      DTS=DX/VA
      DT=SN*DTS
      TA2=NA*DTS/2.
      DT2=DT*DT
      WR2=0.5*K0*VA*VA/R0
      AMDA =6.2831854/K0
      W=WR2*NA*DTS
      T1=6.2831854/W
      TR=DT/T1
      APL=DX*NA/2.
      THETA=ATAN2(APL,R0)
      APL=2.*APL
      WD=VA*SIN(THETA)/AMDA
      TD1=6.2831854/WD
```

UNCLASSIFIED

```
      TRD=DT/TD1
      PRINT 15, NA,KL,VA,RO,AMDA
   15 FORMAT(* CALCULATION OF SCATTERING FROM A SET OF*I4,*DISCRETE SCAT
     1TERERS WITH*I4,*LOOKS,VELOCITY VA=*E10.3 /* RANGE=*E10.3,*WAVELENG
     2TH =*E10.3)
      PRINT 16, DT,DTS,W,T1,TR,APL,THETA,WD,TD1,TRD
   16 FORMAT(* TIME BETWEEN LOOKS DT=*E10.3,*TIME REQUIRED TO TRAVEL THE
     1 SPACING BETWEEN SCATTERERS=*E10.3/* HIGHEST FREQ. W AND PERIOD T1
     2 OF THE SCINTILLATING SIGNAL=*E10.3,*,*E10.3,*RATIO DT/T1 =*E10.3/
     3* SYNTHETIC APERATURE LENGTH=*E10.3,* BEAM WIDTH=*E10.3/* HIGHEST
     4DOPPLER FREQ.=*E10.3,* DOPPLER PERIOD TD1=*E10.3,* RATIO DT/TD1=*
     5E10.3)
      DO 1 K=1,KL
      C(K)=(0.,0.)
      NS1=SN*(K-1)+1
      NS2=NA+NS1-1
      DO 2 I=NS1,NS2
      ANGLE=RANF(-1)-0.5
      PHI=((K-1)*DT-I*DTS+TA2)**2
      II=I
      IF(II .GT. NTS) II=II-NTS
      ANGLE=0.
      PHASE=6.283184*ANGLE
      IF(II .EQ. 6) PHASE=0.
      IF(II .EQ. 5) PHASE=0.
      PI=(-WR2*PHI+PHASE)*CMPLX(0.,1.0)
    2 C(K)=C(K)+A(II)*CEXP(PI)
      CN(K)=C(K)
      CK=C(K)
      RC(K)=REAL(CK)
      DC=CK*CONJG(CK)
      D(K)=REAL(DC)
      DK=D(K)
    1 C(K)=C(K)/SQRT(DK)
      DO 4 K=1,KM
      PHI=(K-1)*DT-TA2
      PHI=WR2*(PHI**2)
      PI=PHI*CMPLX(0.,1.0)
    4 CM(K)=CEXP(PI)
      DO 5 K=1,KL
      CPN=(0.,0.)
      CPM=(0.,0.)
      DO 19 L=1,KM
      LK=K+L-1
      IF(LK .GT. KL) LK=LK-KL
      CPM=CPM+CN(LK)*CM(L)
   19 CPN=CPN+C(LK)*CM(L)
      MN(K)=CABS(CPM)
```

```
    5 M(K)=CABS(CPN)
      PRINT 10
   10 FORMAT(* THE NUMERATOR CN(K) IS*)
      KS=(KL+1)/NA+1
      KU=KS+9
      PRINT 17,(CN(K),K=1,10),(CN(K),K=KS,KU)
   17 FORMAT(20(1H ,5(C(E10.3,E10.3),1X)/))
      PRINT 13
   13 FORMAT(* THE SQUARE OF D(K) IS*)
      PRINT  7,( D(K),K=1,10),( D(K),K=KS,KU)
      PRINT 12
   12 FORMAT(* THE MAP FUNCTION IS*)
    7 FORMAT(10(1H ,10E10.3/))
      CALL PLOT(M,KL,3,1)
      CALL PLOT(MN,KL,3,1)
      END
      SUBROUTINE PLOT(A,KL,IW,IA)
      DIMENSION A(KL),LINE(121)
      INTEGER BLANK,DOT,STAR,PAREN,COM
      DATA(NA=121),(BLANK=1H ),(DOT=1H.),(STAR=1H*),(PAREN=1H'),(COM=1H,
     1)
      G=120./IA
      G1=1.5+(IA-1)*60.
      IC=G1
      B=0.
      DO 13 I=1,KL
      AA=A(I)
      AA=ABS(AA)
   13 B=AMAX1(AA,B)
      DO 1 I=1,NA
    1 LINE(I)=DOT
      GO TO (2,3,4),IW
    2 PRINT 100
      GO TO 10
    3 PRINT 101
      GO TO 10
    4 PRINT 102
   10 PRINT 105,LINE
      DO 90 J=1,KL
      DO 12 I=1,NA
   12 LINE(I)=BLANK
      LINE(IC)=DOT
      IP=G1+G*A(J)/B
      LINE(IP)=STAR
   90 PRINT 105,LINE,A(J)
  100 FORMAT(1H1,* PLOT OF PHASE C(K)*)
  101 FORMAT(1H1,* PLOT OF THE MATCHED FILTER RESPONSE TO THE RESULTANT
     1SIGNAL*)
  102 FORMAT(1H1,* PLOT OF MAPPING FUNCTION*)
  105 FORMAT(1H ,121A1 ,2X,E10.3)
      RETURN
      END
         SCOPE
'LOAD
'RUN,5,1200
''GG
```

Security Classification

UNCLASSIFIED

DOCUMENT CONTROL DATA - R & D

(Security classification of title, body of abstract and indexing annotation must be entered when the overall report is classified)

1. ORIGINATING ACTIVITY *(Corporate author)*

Naval Research Laboratory
Washington, D.C. 20375

2a. REPORT SECURITY CLASSIFICATION

UNCLASSIFIED

2b. GROUP

3. REPORT TITLE

Resolution of Point Scatterers by Hard-Limited Synthetic Aperture Radar

4. DESCRIPTIVE NOTES *(Type of report and inclusive dates)*

Final report on one phase of a continuing NRL Problem

5. AUTHOR(S) *(First name, middle initial, last name)*

George C. Georges

6. REPORT DATE

June 25, 1973

7a. TOTAL NO. OF PAGES

32

7b. NO. OF REFS

12

8a. CONTRACT OR GRANT NO.

NRL Problem R07-02

b. PROJECT NO.

RR 021-01-41-5550

c.

d.

9a. ORIGINATOR'S REPORT NUMBER(S)

NRL Report 7566

9b. OTHER REPORT NO(S) *(Any other numbers that may be assigned this report)*

10. DISTRIBUTION STATEMENT

Approved for public release; distribution unlimited.

11. SUPPLEMENTARY NOTES

12. SPONSORING MILITARY ACTIVITY

Department of the Navy
Office of Naval Research
Arlington, Va. 22217

13. ABSTRACT

Image maps of collections of point targets are investigated for hard-limited synthetic aperture radar application. Some aspects of hard-limiting, such as image suppression and spurious image generation, are derived under specialized weak-scatterer assumptions. Also, the effect of random variations of target phases on synthetic aperture resolution are studied. Such phase deviations are used to model random motions of target locations and, as expected, it is found that they hinder one's ability to resolve the targets. Graphical plots of some point-target arrangements are presented to illustrate effects of hard limiting and random phase variations. Numerical calculations are used to verify the approximate weak-scatterer theory and to study more general cases such as problems involving more than one strong target which are not readily solved by analytical means.

A simple averaging procedure is devised which predicts many aspects of the more accurate numerical results, and the procedure may perhaps be employed in future investigations of mapping continuum scattering surfaces rather than point scatterers.

DD FORM 1 NOV 65 1473 (PAGE 1)

S/N 0101-807-6801

Security Classification

Security Classification

14. KEY WORDS	LINK A ROLE	LINK A WT	LINK B ROLE	LINK B WT	LINK C ROLE	LINK C WT
Hard-limited radar maps						
Spurious target generation by radar						
Synthetic aperture radar						
Oil-spill detection over water by radar						

DD FORM 1 NOV 65 1473 (BACK)
(PAGE 2)

Security Classification

☆U.S. GOVERNMENT PRINTING OFFICE:1973 542-163/Z-3 1-3